[AMERICAN JOURNAL OF SCIENCE, VOL. 289, JANUARY, 1989, P. 1–16]

American Journal of Science

JANUARY 1989

LOW PRESSURE LIQUIDUS RELATIONS IN THE SYSTEM Mg_2SiO_4–Ca_2SiO_4–$NaAlSiO_4$–SiO_2

VIVIAN PAN AND JOHN LONGHI*
Department of Geology and Geophysics, Yale University,
New Haven, Connecticut 06511

ABSTRACT. New one atmosphere data from melting experiments are presented in the system Mg_2SiO_4 (Fo)–Ca_2SiO_4 (La)–$NaAlSiO_4$ (Ne)–SiO_2 (Sil). Electron microprobe analyses of quenched liquids and coexisting mineral phases are used to construct liquidus diagrams for forsterite and nepheline saturation surfaces. Melting experiments have located the temperature maximum along the forsterite–diopside–nepheline cotectic (M, 1160 ± 3°C) and the peritectic involving forsterite + diopside + nepheline + melilite + liquid (I, 1150 ± 3°C). At peritectic I, forsterite is in reaction with liquid to form diopside, nepheline, and melilite. The phase equilibria in this system are appropriate analogs for those encountered by very alkaline magmas such as basanites, tephrites, nephelinites, and melilitites.

INTRODUCTION

Alkalic basaltic rocks are silica-undersaturated volcanic rocks that include alkali olivine basalts, basanites, tephrites, nephelinites, and melilitites. The common associated minerals are olivine, augite, plagioclase, nepheline, and melilite. Analogs of the liquidus equilibria of these basaltic rocks are present in the system Mg_2SiO_4 (Fo)–Ca_2SiO_4 (La)–$NaAlSiO_4$ (Ne)–SiO_2 (Sil) which is an expansion of the basalt tetrahedron Forsterite–Diopside–Nepheline–Silica of Yoder and Tilley (1962). This system contains liquid compositions in equilibrium with the common minerals of alkalic basaltic rocks and is therefore an essential starting point to study the phase equilibria of silica-undersaturated volcanic rocks.

Schairer and Yoder (1964) experimentally determined the liquidus equilibria along six planes Ne–Ak–Di, Ne–Ak–Wo, Ab–Wo–Ak, Ab–Ak–Di, Ne–Ak–Ab, and Ne–Wo–Di (abbreviations in app. I) within the Fo–La–Ne–Sil system (fig. 1). A significant outcome of this study was the construction of a flow sheet for liquid trends in the system. Much of the present experimental work was guided by this earlier study.

Onuma and Yagi (1967) reinvestigated the plane Ne–Ak–Di and rendered conclusions similar to Schairer and Yoder (1964). Other important works include those of Schairer and Yoder (1960, 1961) in

* Present address: Lamont-Doherty Geological Observatory, of Columbia University, Palisades, New York 10964

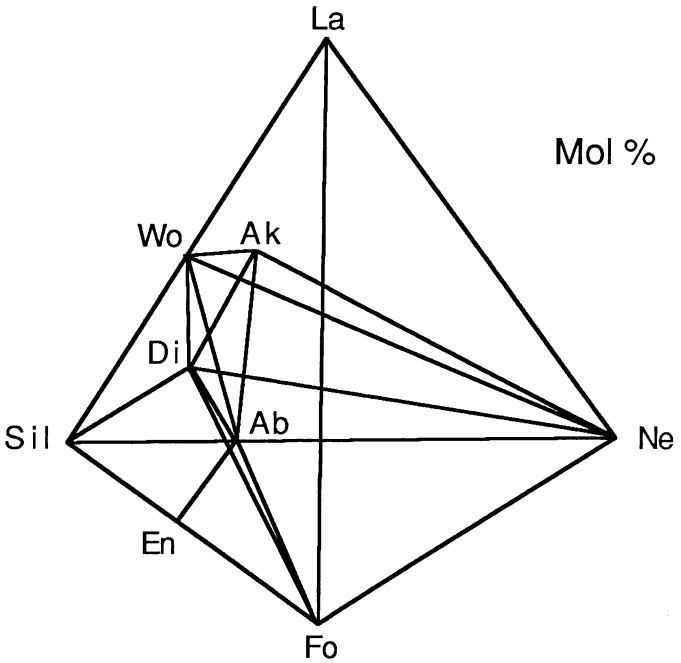

Fig. 1. The expanded basalt tetrahedron after Schairer and Yoder (1964) displaying the planes that have been previously studied: Ne–Ak–Di, Ne–Ak–Wo, Ab–Wo–Ak, Ab–Ak–Di, Ne–Ak–Ab, Ne–Wo–Di, Ne–Di–Sil, and Ne–Fo–Sil.

which they determined phase equilibria in the planes Ne–Di–Sil and Ne–Fo–Sil. Biggar and Humphries (1981) experimented in the plane Fo–Di–Pl where the Pl component of the liquid ranged from An_{100} to An_{33}. Although they did not include the endmember Ab component, the position of the fo–di–ab liquidus can be extrapolated from their data.

All the authors mentioned above constructed their phase diagrams from the liquidus relations of selected bulk compositions. The general liquidus topology was established, but as with other pre-microprobe studies, quantitative analyses of coexisting crystals and quenched liquids and precise determination of invariant points were not possible. As crystallization proceeds, liquid compositions move away from their initial bulk compositions; therefore, it is necessary to document the actual compositions of the multi-saturated liquids. Electron microprobe analyses of quenched liquids and their equilibrium mineral assemblages are necessary for the discussion of reaction relationships and liquidus equilibria.

Sack, Walker, and Carmichael (1987) presented an experimental study of natural alkalic lavas in which the plagioclase-saturated liquidus

surface was projected onto the Ol–Di–Ne plane. The alkalic lavas extend to very K-rich compositions where leucite-saturated liquidus equilibria were involved. Our study differs from Sack, Walker, and Carmichael in that we aim to establish a framework for understanding a wider range of liquidus relations that includes plagioclase-absent equilibria. The motivation for this approach is to understand the fundamental liquidus topology in the simple system in preparation for more complex studies (such as the effects of varying the Ab/(Ab + An) ratio on liquidus boundaries).

This paper augments the previous works through the construction of pseudo-ternary liquidus diagrams from electron microprobe anlayses of experimental quenched liquids and their equilibrium crystals in the system Fo–La–Ne–Sil. We will discuss the liquidus equilibria in the silica-undersaturated portion of the expanded basalt tetrahedron and their implications for the petrology of alkalic basaltic rocks.

EXPERIMENTAL METHODS

Glass compositions that contain Na_2O in significant concentrations need careful preparation due to the volatility of Na_2O at high temperatures. A sodium silicate glass of 70 wt percent SiO_2 and 30 wt percent Na_2O was first prepared as described by Schairer and Bowen (1956). The remaining dried oxides MgO, Al_2O_3, SiO_2, and $CaCO_3$ were mixed together with the sodium silicate glass in a Pt crucible. The Pt crucible was placed in a furnace at 1000°C overnight for decarbonization. The sample was fused in a Deltech furnace at approx 1350°C for 2 hrs and then quenched in water. The latter process was carried out two to three times with crushing inbetween to homogenize the glass. A magnet was used to remove any added metal chips during crushing. The homogeneity of the glass was checked under an optical microscope with oils of known refractive indices.

The synthesized starting glass compositions (table 1) were loaded into Pt capsules that were sealed with a H_2-O_2 torch at both ends to minimize Na_2O loss during the experiment (electron microprobe analy-

TABLE 1

Starting glass compositions for experiments

	A7P0	A10P0	A13P0	A14P0	A16P0	A17P0	A19P0	A22P0	A23P0	A24P0
Wt %										
SiO2	58.36	56.72	55.59	54.99	51.99	51.32	50.19	51.66	51.33	63.67
Al2O3	20.95	20.17	20.02	21.13	18.45	19.97	17.74	16.68	17.73	18.53
MgO	3.76	5.79	6.33	5.22	9.51	8.13	10.36	10.42	9.14	4.18
CaO	4.19	5.04	5.87	5.81	8.82	8.71	10.18	11.09	11.02	2.33
Na2O	12.73	12.26	12.17	12.84	11.21	12.03	10.78	10.14	10.77	11.27
Oxy %										
Fo	6	10	11	9	17	14	18	18	16	7
La	5	6	7	7	11	11	13	14	14	3
Ne	56	54	54	57	51	55	50	46	49	48
Sil	33	30	28	27	21	20	19	22	21	42

ses of enclosed glass showed no detectable Na_2O loss during fusion). Thermocouples of Pt94–Rh6/Pt70–Rh30 were calibrated against gold (1064°C) and lithium disilicate (1208°C). The Pt capsules were suspended in a Deltech furnace first at 50°C below the desired temperature for 3 days to promote nucleation, then raised to the desired liquidus temperature for 7 days. After a total of 10 days, the samples were dropped and quenched in water. Temperature fluctuations during the experimental period are less than ±2°C.

The experimental products were first examined in oil under the optical microscope and then mounted into epoxy for polish, reflected light microscopy and electron microprobe analysis. Electron microprobe analyses were performed at Lamont-Doherty Geological Observatory on the Cameca CAMEBAX/MICRO wave dispersive system at 5ηA sample current and 15kV accelerating voltage. To minimize Na_2O loss during probing, the beam was set on small raster mode with a beam area of 144×10^{-12} m^2 for 20 sec counting time for Na_2O. Amelia Albite was the standard for Na_2O, Al_2O_3, and SiO_2. The remaining oxides, MgO and CaO, were standardized against glasses prepared by Dalheim (1977).

TABLE 2

Experimental conditions, duration and products

Run #	T°C	Time (hrs)	Products
A7P0-2	1100	168	gl, fo, di, ne
A10P0-1	1148	211	gl, fo, di
A10P0-2	1138	170	gl, fo, di
A10P0-3	1130	192	gl, fo, di
A13P0-1	1150	189	gl, fo, di
A13P0-2	1138	170	gl, fo, di
A13P0-3	1130	192	gl, fo, di, ne
A14P0-1	1150	189	gl, fo, di
A14P0-2	1138	170	gl, fo, di, ne
A14P0-3	1130	192	gl, fo, di, ne
A16P0-1	1175	293	gl, fo
A16P0-2	1165	187	gl, fo, di
A16P0-3	1155	140	gl, fo, di, ne
A17P0-1	1175	293	gl, fo
A17P0-2	1165	187	gl, fo, ne
A17P0-3	1155	140	gl, fo, ne, di
A19P0-1	1185	170	gl, fo
A19P0-2	1165	187	gl, fo, ne, mel
A22P0-1	1160	96	gl, fo, di, mel
A23P0-1	1160	96	gl, fo, mel
A23P0-2	1150	189	gl, fo, mel, di, ne
A24P0-2	1150	189	gl, fo, di

EXPERIMENTAL RESULTS

Table 2 is a summary of the experiments performed. Compositions very low in La component produced quench crystals, therefore we were unable to locate the plagioclase saturation surface. At higher La component compositions, however, euhedral to subhedral crystals formed resembling those in figure 2. We interpret these crystalline textures as equilibrium phases. Reversal experiments in this region were not performed because of the observed textures and the consistency among liquid lines of descent and coexisting mineral compositions. Electron microprobe data of experimental liquids and coexisting mineral phases are given in table 3. Here we report liquid compositions that are saturated with two or more crystalline phases. The experiments were designed to produce forsterite-saturated liquids, therefore, all reported liquids have forsterite as a crystalline phase. Some of the mineral phases (except forsterite) were not analyzed due to their extreme small size ($<3 \times 10^{-6}$ m). Forsterite was not analyzed routinely because it admits a limited range of solid solution (approx 1 percent La). We will discuss later, however, solid solution of the other mineral phases as an important aspect of the phase equilibria.

In order to present the data in a systematic fashion, the oxide compositions are recast into two pseudo-ternary diagrams where the units are volume-conservative oxygen units as described by Longhi and

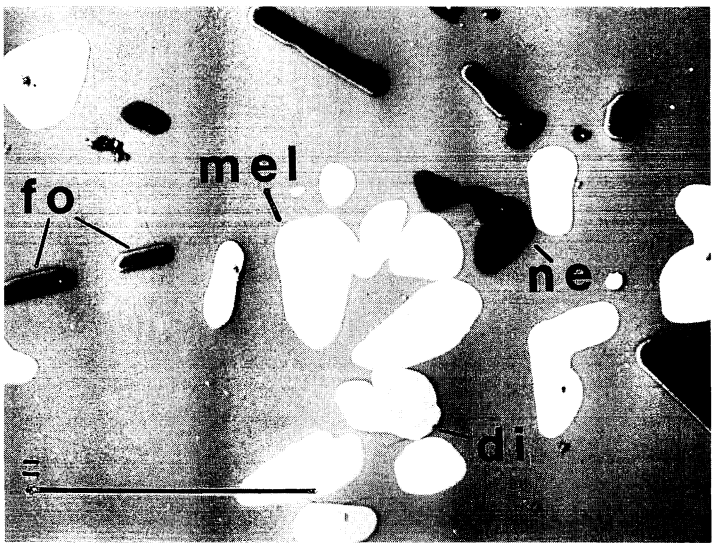

Fig. 2. Back scatter SEM photomicrograph of invariant assemblage forsterite + diopside + melilite + nepheline + liquid at 1150 ± 3°C (Run A23PO-2). The bar denotes 100 microns.

TABLE 3

Electron microprobe analyses of selected forsterite saturated assemblages

	A19P0-2			A22P0-1			A23P0-1		A16P0-3			
Phase	gl	ne	mel	gl	di	mel	gl	mel	gl	ne	di	fo
SiO2	50.65	44.71	44.84	50.82	54.59	44.21	50.50	44.14	51.65	45.22	55.55	42.54
Al2O3	19.52	33.24	7.48	18.95	1.37	6.91	19.44	7.19	20.73	33.75	2.04	0.06
MgO	6.17	0.46	9.30	6.92	18.67	9.93	6.56	9.82	5.43	0.31	18.21	56.51
CaO	8.99	2.25	33.29	10.67	25.15	35.28	10.14	34.90	8.20	2.46	25.15	0.77
Na2O	13.83	18.51	4.26	13.04	0.28	4.00	13.14	4.12	13.30	18.25	0.32	0.01
Total	99.16	99.17	99.17	100.40	100.06	100.33	99.78	100.17	99.31	99.99	101.30	99.90
Oxygen		4	7		6	7		7		4	6	4
Si		1.057	1.996		1.965	1.97		1.968		1.058	1.97	0.999
Al		0.926	0.392		0.058	0.363		0.378		0.931	0.085	0.002
Mg		0.016	0.617		1.002	0.66		0.653		0.011	0.965	1.979
Ca		0.057	1.618		0.97	1.684		1.667		0.062	0.956	0.019
Na		0.848	0.368		0.02	0.346		0.356		0.828	0.022	0
Total		2.904	4.991		4.015	5.023		5.022		2.89	3.998	2.999
Other Phases		fo			fo			fo				

	A17P0-3				A23P0-2					A10P0-2	A14P0-2		A14P0-3	A7P0-2
Phase	gl	ne	di	fo	gl	ne	di	mel	fo	gl	gl	di	gl	gl
SiO2	51.05	45.92	55.23	42.81	51.41	46.41	54.98	44.60	43.01	62.48	54.27	55.31	54.55	56.20
Al2O3	20.24	32.61	1.29	0.06	20.00	32.57	1.62	7.84	0.07	18.71	21.67	1.90	22.03	22.72
MgO	5.80	0.72	18.56	56.28	6.00	0.60	18.25	9.11	56.20	3.27	4.28	18.48	4.25	3.02
CaO	8.89	2.43	25.05	0.81	8.77	2.26	24.81	34.05	0.83	2.52	5.61	24.32	4.51	2.93
Na2O	13.50	18.16	0.35	0.03	13.71	18.22	0.38	4.39	0.02	13.10	14.39	0.40	14.26	14.86
Total	99.48	99.84	100.48	100.00	99.89	100.06	100.04	99.99	100.14	100.08	100.02	100.41	99.60	99.73
Oxygen		4	6	4		4	6	7	4			4		
Si		1.076	1.977	1.004		1.083	1.976	1.984	1.007			1.976		
Al		0.9	0.054	0.002		0.896	0.069	0.411	0.002			0.08		
Mg		0.025	0.991	1.968		0.021	0.978	0.604	1.962			0.984		
Ca		0.061	0.961	0.02		0.057	0.955	1.623	0.021			0.931		
Na		0.825	0.024	0		0.825	0.026	0.379	0.001			0.028		
Total		2.887	4.007	2.994		2.882	4.004	5.001	2.993			3.999		
Other phases										fo,di	fo,ne		fo,di,ne	fo,di,ne

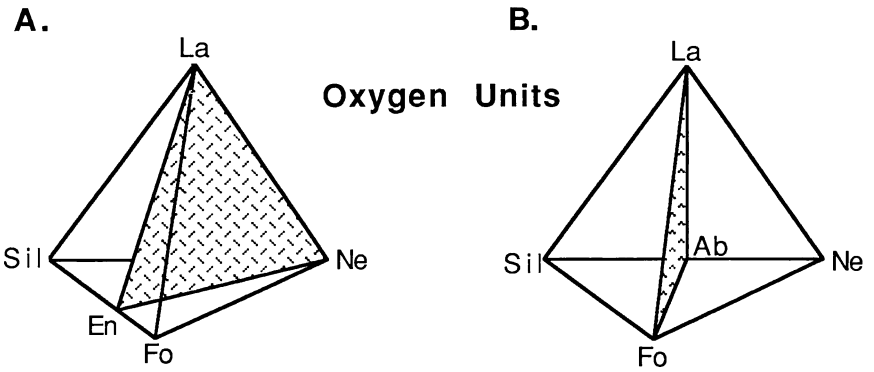

Fig. 3. The graphical method used to illustrate liquidus equilibria in the expanded basalt tetrahedron in oxygen units. (A) The projection from the Fo component for forsterite saturated liquidus surfaces onto the plane En–La–Ne. (B) The projection from the Ne component for nepheline saturated liquidus surfaces onto the plane Fo–La–Ab. Projection equations are given in the appendix.

Pan (1988). Three-dimensional liquidus surfaces saturated with forsterite are projected from the Fo component onto the plane En–La–Ne (fig. 3A); liquidus surfaces saturated with nepheline are projected from the Ne component onto the plane Fo–La–Ab (fig. 3B, equations are given in app.). These two projection schemes bisect the tetrahedron and illustrate the liquidus equilibria of the silica-undersaturated volume from two perspectives. In contrast to the graphical methods of Schairer and Yoder (1964) that illustrate the liquidus equilibria along several ternary joins in the system, the projection method gives a more comprehensive view of the topology in the system.

The pseudo-ternary liquidus diagrams are illustrated in figures 4 and 5. Because our experiments concentrate on defining the forsterite-saturated liquidus, the Fo projection is perhaps the most useful diagram in discussing phase equilibria. In fact, the Fo projection diagram can be read much as one would read a simple ternary diagram due to the relatively pure composition of the projection phase. The Fo projection, however, cannot reveal reaction relationships involving forsterite, and this projection alone is not suitable for discussion of all the topologies in the system. The Ne projection is effective for illustrating the liquidus relationships behind the saturation surface of forsterite, but a note must be made regarding the pitfalls of this projection. Unlike the Fo projection, the diagram in figure 4 cannot be read as a simple ternary diagram due to extensive solid solution in the projection phase. The nepheline saturated liquidus is projected from the position of the stoichiometric Ne component rather than from the actual compositions of the liquidus nephelines; therefore, direct estimates regarding the odd or even nature of the univariant curves and peritectic or eutectic character of invariant points cannot be made. Nevertheless, the Ne

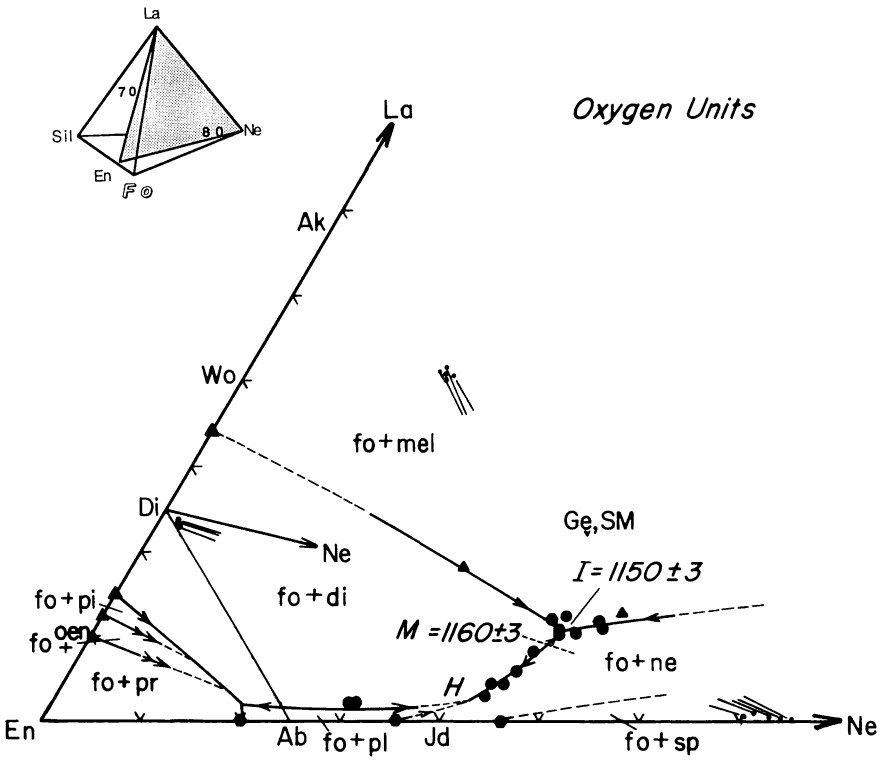

Fig. 4. The forsterite saturation surface projected from the Fo component onto the En–La_{70}–Ne_{80} portion of the plane. Large solid circles are multiply saturated experimental liquids from this study. Small solid circles with tie lines are compositions of mineral phases in equilibrium with the multiply saturated liquids. Solid hexagons are data taken from Schairer and Yoder (1961) in the system Nepheline–Forsterite–Silica. Solid triangles are data from Onuma and Yagi (1967), Kushiro (1972), and Longhi and Boudreau (1980). Univariant curves with single arrows indicate cotectics and double arrows indicate peritectics. Dashed curves are approximations where data are not available. Thermal maximum M (1160 ± 3°C) is coplanar with solid solution compositions of diopside and nepheline and relatively pure forsterite. Invariant assemblage fo + di + mel + ne + l (1150 ± 3°C) is denoted by I.

projection does serve to illustrate the relative positions of the liquidus volumes behind the saturation surface of forsterite. The reaction relationships of forsterite can be determined by graphical methods such as an additional projection from the La component or by the calculation method of Korzhinskii (1959) and Presnall (1986) which describes compositional relationships in multi-component systems.

Solid solution.—With the exception of forsterite, the mineral phases have significant solid solution. The mineral compositions of liquidus assemblages near points I and M are plotted on the projection diagrams of figures 4 and 5 with partial tie lines directing toward their equilibrium liquid compositions. Diopside plots off its stoichiometric composition

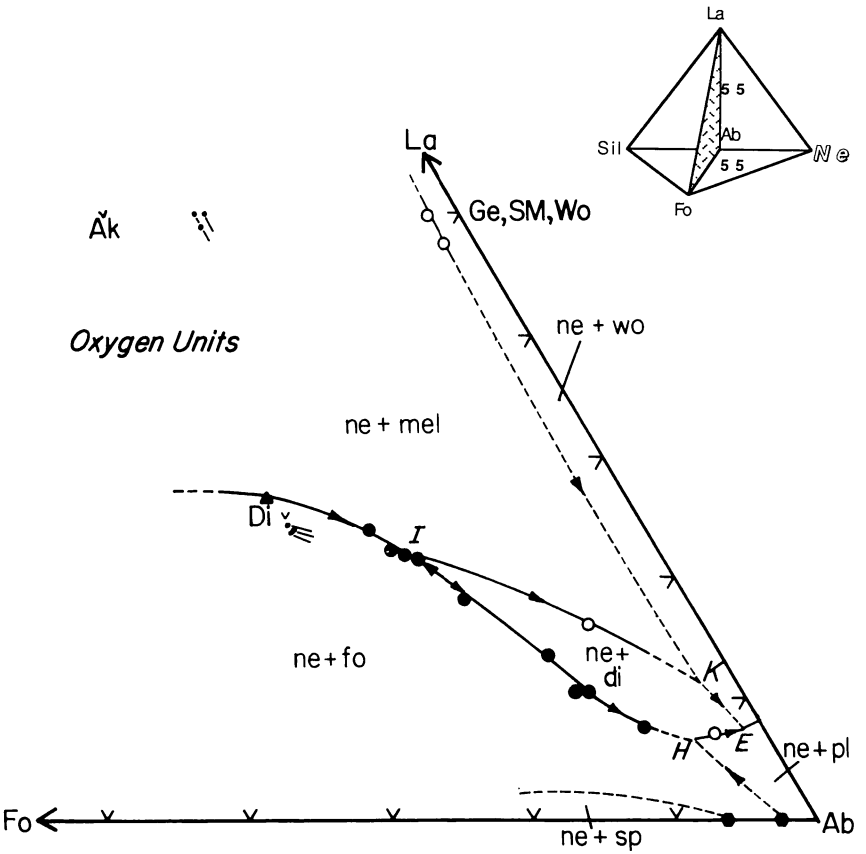

Fig. 5. The nepheline saturation surface projected from the Ne component onto the Fo_{55}–La_{55}–Ab portion of the plane. Symbols are the same as in figure 4. Open circles are data from Schairer and Yoder (1964) along the joins Ne–Ak–Ab, Ne–Ak–Wo, and Ne–Wo–Di.

due to solid solution with the $CaAl_2SiO_6$ (CaTs), and $NaAlSi_2O_6$ (jadeite) components. Melilites are solid solutions of the endmembers $Ca_2MgSi_2O_7$ (akermanite), $NaCaAlSi_2O_7$ (soda-melilite), and $Ca_2Al_2SiO_7$ (gehlenite) with proportions averaging 60:38:2. The melilites also contain minor excesses of magnesium and silicon; hence, they plot slightly off the Ak-Ge-SM join. Liquidus nepheline compositions are plotted in figure 6 as well as in figure 4. These experimental nepheline compositions plot far off the stoichiometric composition due to solid solution with excess magnesium and silicon. The projection of figure 6 clearly demonstrates the substitution of $Mg^{2+} + Si^{4+}$ for $2Al^{3+}$ in the form of a $Na_2MgSi_3O_8$ component. Minor amounts of calcium are also in solid solution with nepheline in the form of $Ca_3Al_2SiO_8$.

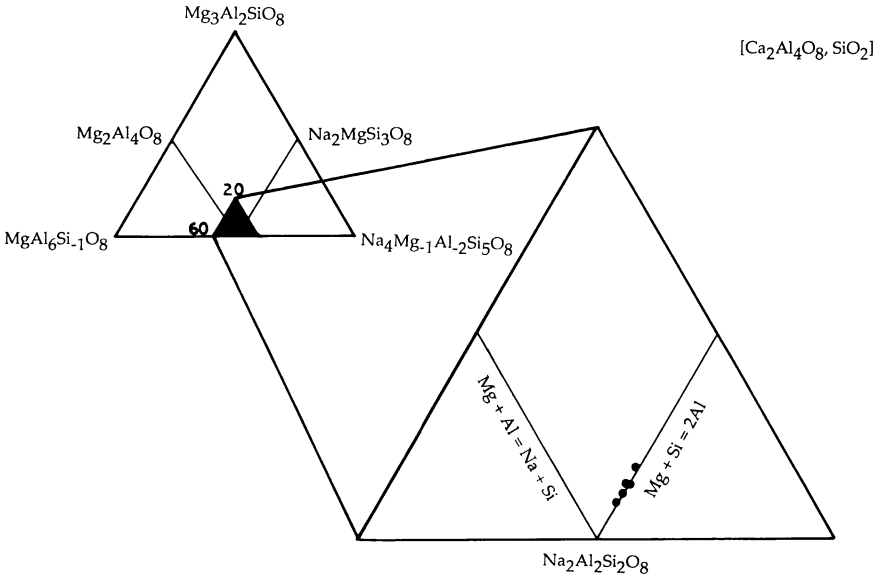

Fig. 6. The projection of liquidus nepheline compositions from $[Ca_2Al_4O_8, SiO_2]$ onto the join $MgAl_6Si_{-1}O_8$–$Mg_2MgAl_2SiO_8$ –$Na_4Mg_{-1}Al_{-2}Si_5O_8$. The enlarged diagram is the filled field shown in the inset.

Phase equilibria.—The Fo projection (fig. 4) illustrates that the critical plane of silica-undersaturation (line Di-Ab) lies very close to the trace of the thermal divide (Yoder and Tilley, 1962; Biggar and Humphries, 1981). Liquids saturated with forsterite, diopside, and plagioclase cannot fractionate across the plane Fo–Di–Ab. Compositions that are hypersthene normative will move down temperature toward the fo + di + pr + pl + l peritectic, and compositions that are nepheline normative will move down temperature toward the fo + di + pl + ne + l (H) peritectic. The position of the fo + di + pl liquidus is interpolated from the study of Biggar and Humphries (1981). The invariant points fo + pr + ab + l, fo + ab + ne + l, and fo + ne + sp + l are from the data of Schairer and Yoder (1961). Our discussion here will be directed toward the phase equilibria on the silica-undersaturated side of the Fo–Di–Ab thermal divide because it is these equilibria that control crystallization of alkalic basalts.

Our experiments indicate that the fo + pl liquidus volume is very limited in composition. We were unable to crystallize equilibrium fo + pl + l assemblages. We were able to produce fo + di + l assemblages, however, in liquids with low La component compositions close to the plagioclase saturation surface. The composition of these liquids constrains the position of the fo + pl liquidus surface. The fo + di + ne + l cotectic has a temperature maximum (M) at 1160 ± 3 °C coplanar with

the solid solution compositions of coexisting forsterite, diopside, and nepheline. The compositions of minerals in equilibrium with liquid near M are given in table 3 under A16PO-3 and A17PO-3. Liquids will move down temperature to invariant point fo + di + pl + ne + l (H) or fo + di + mel + ne + l (I) depending on whether their composition projects below or above the plane of coexisting fo + di + ne. The univariant curves fo + di + mel + l and fo + mel + ne + l converge with decreasing temperature to the fo + di + mel + ne + l (I) invariant assemblage (1150 ± 3°C). None of our experiments produced the fo + sp assemblage, and we interpret the fo + sp liquidus surface to be relatively small compared to the fo + ne liquidus surface. The estimated position of the fo + ne + sp liquidus curve, shown as a dashed line, is constrained only by the composition of one fo + ne + sp liquidus assemblage from Schairer and Yoder (1961).

Figure 7 is a schematic projection of the compositions of coexisting crystals and liquid at invariant point I (1150 ± 3°C) from the La component onto the base of the expanded tetrahedron. This diagram illustrates that the composition of the liquid lies outside the volume bounded by the compositions of the crystalline phases and that the tie line joining liquid and forsterite pierces the compositional plane of ne–mel–di. This relationship requires that forsterite be in reaction with liquid at invariant point I. In addition, we utilized the algebraic method of Presnall (1986) to determine the mass balance relationships among

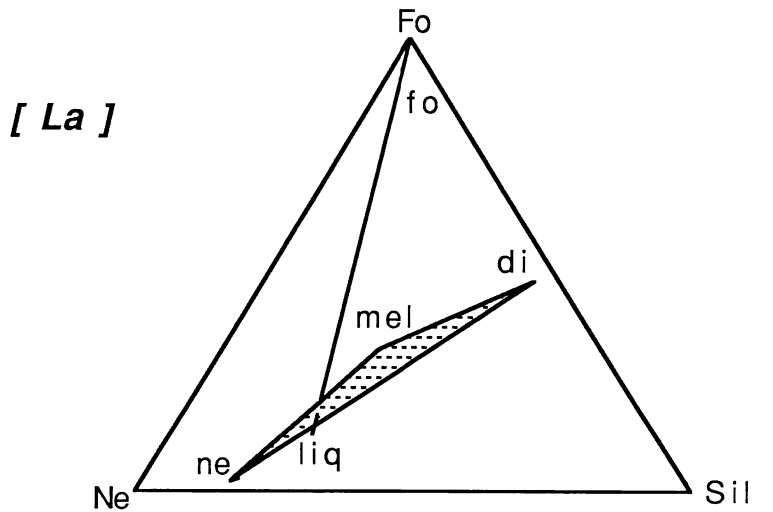

Fig. 7. The projection from the La component onto the plane Fo–Ne–Sil for invariant point I (fo + di + mel + ne + l, 1150 ± 3°C). The liquid composition lies outside the compositional volume of its coexisting minerals phases. A tie line joining forsterite and liquid pierces the ne + di + mel plane indicating the reaction: fo + l → ne + di + mel.

the coexisting phases at I. These calculations agree with the graphical analysis and require the following equilibrium at invariant point I:

$$fo + l = di + mel + ne.$$

As mentioned earlier, our experiments were unsuccessful in producing plagioclase-saturated liquids. Consequently, we are unable to locate the composition of point H (fo + pl + ne + di + l) precisely, and hence, we cannot be certain of the equilibrium relationships. Nevertheless, inspection of figures 4 and 5 in conjunction with estimate calculations suggest that H is also a quaternary peritectic with forsterite in reaction with liquid in agreement with Schairer and Yoder (1960, 1964).

The Ne projection in figure 5 illustrates the nepheline-saturated liquidus surfaces in Fo–La–Ne–Sil. This projection is similar to the one depicted by Yoder (1979, fig. 13-4) except we have included new experimental data to display the positions of invariant point I and the fo + di + ne + l boundary. The univariant curves fo + mel + ne + l, fo + di + ne + l, and fo + pl + ne + l are the same as those in the Fo projection; however, there are forsterite-absent surfaces and univariant curves not evident in figure 4. In general, from this perspective, we see that as Ab component increases, the forsterite saturated liquidus surface contracts. More specifically, the fo–di–ne thermal divide causes liquids to fractionate into two general crystallization paths. In the first case, liquids saturated with fo + ne + mel or with fo + ne + di but lying on the high-La side of the fo–di–ne thermal divide will first encounter invariant point I. After fo is completely consumed at I, fractionating liquids will move down the ne + di + mel + l cotectic to reach invariant point K (ne + di + mel + wo + l) where wollastonite begins to crystallize and melilite begins to dissolve. After melilite is consumed, the liquid will proceed toward the eutectic E where plagioclase joins diopside, wollastonite, and nepheline. In the second case, liquids saturated with fo + di + ne that are on the low-La side of the fo–di–ne thermal maximum will fractionate to invariant point H (fo + di + pl + ne + l). Similarly, liquids saturated with fo + pl + ne will evolve to H. As discussed above, forsterite appears to be in reaction with liquid at H, so that upon consumption of forsterite the residual liquid will crystallize diopside, nepheline, and plagioclase until it reaches eutectic E.

DISCUSSION

Petrologists have long utilized the liquidus relations of simple oxide systems as useful analogs of the liquidus relations of more complex natural magmas. Liquidus equilibria of tholeiitic basalts can be modelled in the silica-rich portion of the four oxide system $CaO–MgO–Al_2O_3–SiO_2$ (CMAS) largely because the major missing natural components, FeO and Na_2O, do not produce additional silicate phases at natural concentration levels and tend to offset one another by shifting most CMAS liquidus boundaries in opposite directions (Longhi, 1987). Alkali

basalts, however, have nepheline as an important phase, hence a minimum of five oxides, Na_2O–CaO–MgO–Al_2O_3–SiO_2 (NCMAS), is necessary to model their phase equilibria. We have represented compositions in this system in terms of the components Fo–La–Ne–Sil (Schairer and Yoder, 1964) which is an expansion of the basalt tetrahedron of Yoder and Tilley (1962). In this four component system the normative feldspar is pure albite, although plagioclases do contain a few percent An component. Relative to the CMAS system, the effects of such highly alkaline compositions are the displacement of liquidus surfaces toward the silica-undersaturated portion of the tetrahedron and the replacement of spinel by nepheline as the major low-silica phase.

Figure 4 illustrates the petrologically relevant portion of the forsterite saturated liquidus surface. This projection clearly shows the fo + di + pl + l temperature maximum to be approximately coincident with the plane Fo–Di–Ab which separates hypersthene normative (tholeiitic) liquid compositions from nepheline normative (alkalic) liquid compositions. In addition, figure 4 shows the incompatibility of sodic-plagioclase and melilite in forsterite saturated liquids due to the fo–di–ne temperature maximum (M) which is in agreement with the conclusions of Schairer and Yoder (1964). Figure 5 shows that this incompatibility extends to forsterite-undersaturated liquids. The implications from these liquidus relationships are not only that tholeiitic and alkalic basalts in general cannot be related by simple crystallization processes, but also, that among alkalic basalts plagioclase-bearing and melilite-bearing varieties cannot be related either.

Schairer and Yoder (1964) predicted a temperature maximum coplanar with Fo–Di–Ne. Electron microprobe analyses of nepheline, diopside, and coexisting liquid, however, demonstrate that the maximum does not lie in the plane of the ideal components. Because nepheline admits MgO, CaO, and excess SiO_2 into solid solution, the position of nepheline plots well off the stoichiometric composition. Diopside contains measurable quantities of CaTs and jadeite molecules and also plots off its stoichiometric composition. As a result of nepheline and diopside solid solution, the coplanarity between coexisting fo, di, ne and l lies well below the trace of the Fo-Di-Ne plane (line from Di to Ne in fig. 4).

Because plagioclase composition varies from intermediate to albitic in the alkalic rock series, it is important to consider the changes in liquidus equilibria produced by varying the proportions of Ab ($NaAlSi_3O_8$) and An ($CaAl_2Si_2O_8$), or, equivalently, Ne ($NaAlSiO_4$) and its Ca-Al analog ($CaAl_2O_4$). For instance, we may expect that the positions of liquidus boundaries appropriate for alkali olivine basalts are slightly different from those of nephelinites because of the different normative plagioclase compositions (Pan and Longhi, 1987). We will treat this phenomenon in a separate paper where we also compare our results to those of Sack, Walker, and Carmichael (1987). For the moment, however, there are some limited but petrologically useful

correlations between natural magmas and the low pressure liquidus equilibria (figs. 4 and 5). Alkali olivine basalts, which commonly have olivine, plagioclase, and augite as both phenocryst and groundmass phases may be thought of as liquids plotting along the fo + di + pl + l cotectic slightly to the Ne-side of the Fo–Di–Ab plane in figure 4. Basanites, which have early olivine, plagioclase, and augite with nepheline in the groundmass, may be thought of as liquids plotting along the fo + di + pl + l cotectic near invariant point H. Tephrites, which are similar to basanites except they lack olivine, may be thought of as liquids that have reacted out olivine at point H and have evolved onto the ne + di + pl + l cotectic in figure 5. Nephelinites have nepheline and augite as phenocrysts ± olivine and ± melilite and may be represented as liquids plotting in the ne + di liquidus field near the peritectic I in figure 5. Most melilitites may be thought of as liquids projecting near the fo + mel + di + l cotectic in figure 4; whereas melilititic-nephelinites project closer to the fo + mel + ne + l cotectic. Both melilititic series should evolve to invariant point I and then lose olivine.

CONCLUSION

The system Fo–La–Ne–Sil is an analog system for the study of alkalic basaltic rocks. The liquidus equilibria within this system span the continuum in composition ranging from hypersthene normative to extremely nepheline normative compositions, and our attention is focused in the nepheline normative portion of the system for alkaline rocks. Pseudo-ternary liquidus diagrams such as the Fo projection and the Ne projection are useful in illustrating the liquidus topology within this system. There exist two thermal divides fo–di–pl (Biggar and Humphries, 1981) and fo–di–ne (1160° ± 3°C): the former separates silica-saturated from silica-undersaturated basalts, and the latter separates plagioclase bearing from melilite bearing lavas. Invariant point I (fo + di + ne + mel + l, 1150° ± 3°C) is a peritectic where forsterite is in reaction with liquid to yield diopside, nepheline, and melilite. Fractionating liquids will terminate at eutectic E (di + ne + wo + pl + l; Schairer and Yoder, 1964). As shown by the fo–di–ne thermal divide, solid solution of mineral phases plays a significant role in the phase equilibria of the system, therefore compositional analysis of the phases is essential. Correlations of these liquidus relationships to natural magmas may be demonstrated for alkali olivine basalts, basanites, tephrites, nephelinites, and melilitites.

ACKNOWLEDGMENTS

We thank S. Bromble for her assistance with the electron microprobe. We also thank Drs. A.D. Edgar, E.F. Osborn, K.E. Windom, and H.S. Yoder for their helpful reviews of the manuscript. This research was supported by NASA grant NAG-9-93.

APPENDIX

I. Abbreviations for components and phases. Capitalized abbreviations denote components and lower case abbreviations denote phases.

Components:

Fo = Mg_2SiO_4	La = Ca_2SiO_4	Ne = $NaAlSiO_4$
Sil = SiO_2	An = $CaAl_2Si_2O_8$	Ab = $NaAlSi_3O_8$
Pl = An + Ab	Di = $CaMgSi_2O_6$	Ak = $Ca_2MgSi_2O_7$
Ge = $Ca_2Al_2SiO_7$	SM = $NaCaAlSi_2O_7$	Wo = $CaSiO_3$
Ol = $(Mg, Fe)_2SiO_4$		

Phases:

fo-forsterite, pr-protoenstatite, oen-orthoenstatite, en-enstatite, di-diopside, mel-melilite, pl-plagioclase, ne-nepheline, sp-spinel, wo-wollastonite, l-liquid.

II. Projection equations are given below where the oxide concentrations are in mole units and the projection coordinates are in oxygen units.

Fo projection:

$La' = [0.5 * (-Al_2O_3 + CaO + Na_2O)] * 4$
$En' = [(SiO_2) + (0.5 * Al_2O_3) - (0.5 * MgO) - (0.5 * CaO) - (2.5 * Na_2O)] * 6$
$Ne', CA' = [(Na_2O) + (Al_2O_3)] * 4$
$Ne' = 2 * (Na_2O)$
$CA' = Al_2O_3 - Na_2O$
Sum = La′ + En′ + Ne′, CA′
substitute:
La = La′/sum
En = En′/sum
Ne, CA = Ne′, CA′/sum

Ne projection:

$Fo' = (0.5 * MgO) * 4$
$La' = [0.5 * (CaO + Na_2O - Al_2O_3)] * 4$
$Pl' = [(0.5 * SiO_2) + (0.25 * \{Al_2O_3 - MgO - CaO\}) - (1.25 * Na_2O)] * 8$
Sum = Fo′ + La′ + Pl′
substitute:
Fo = Fo′/sum
La = La′/sum
Pl = Pl′/sum

La projection:

$Fo' = (0.5 * MgO) * 4$
$Sil' = [SiO_2 + (0.5 * \{Al_2O_3 - MgO - CaO\}) - (2.5 * Na_2O)] * 2$
$Ne', CA' = (Na_2O + Al_2O_3) * 4$
Sum = Fo′ + Sil′ + Ne′, CA′
substitute:
Fo = Fo′/sum
Sil = Sil′/sum
Ne, CA = Ne′, CA′/sum

$Ca_2Al_4O_8$ + SiO_2 projection (mole units):

$MgAl_6Si_{-1}O'_8 = (0.375 * \{Al_2O_3 - CaO\}) + (0.125 * \{Na_2O - MgO\})$
$Mg_3Al_2SiO'_8 = (0.375 * MgO) + (0.125 * \{Na_2O - Al_2O_3 + CaO\})$
$Na_4Mg_{-1}Al_{-2}Si_5O'_8 = 0.5 * Na_2O$
$Ca_2Al_4O'_8 = 0.5 * CaO$
$SiO'_2 = SiO_2 + \{0.5 * (Al_2O_3 - MgO - CaO)\} - \{2.5 * Na_2O\}$
$Sum = MgAl_6Si_{-1}O'_8 + Mg_3Al_2SiO'_8 + Na_4Mg_{-1}Al_{-2}Si_5O'_8$
substitute:
$MgAl_6Si_{-1}O_8 = MgAl_6Si_{-1}O'_8/sum$
$Mg_3Al_2SiO_8 = Mg_3Al_2SiO'_8/sum$
$Na_4Mg_{-1}Al_{-2}Si_5O_8 = Na_4\,Mg_{-1}Al_{-2}Si_5O'_8/sum$

References

Biggar, G. M., Humphries, D. J., 1981, The plagioclase, forsterite, diopside, liquid equilibrium in the system $CaO–Na_2O–MgO–Al_2O_3–SiO_2$: Mineralological Magazine, v. 44, p. 309–314.

Dalheim, P. A., ms, 1977, Calculation of Empirical Coefficients in Multicomponent Oxide Systems for the Reduction of Electron Microprobe Data: M.S. thesis, University of Oregon, Eugene, Oregon.

Korzhinskii, D. A., 1959, Physiochemical basis of the analysis of the paragensis of minerals: New York, Consultants Bureau.

Kushiro, I., 1972, Determinations of liquidus relations in synthetic silicate systems with electron probe analysis: The system forsterite-diopside-silica at 1 atmosphere: Am. Mineralogist, v. 57, p. 1260–1271.

Longhi, John, 1987, Liquidus equilibria and solid solution in the system $CaAl_2\,Si_2O_8–Mg_2SiO_4–CaSiO_3–SiO_2$ at low pressure: American Journal of Science, v. 287, p. 265–331.

Longhi, John and Boudreau, A., 1980, The orthoenstatite liquidus field in the system forsterite-diopside-silica: Am. Mineralogist, v. 64, p. 563–573.

Longhi, John and Pan, Vivian, 1988, A reconnaisance study of phase boundaries in low-alkali basaltic liquids: Jour. Petrology, v. 29, p. 115–148.

Onuma, K. and Yagi, K., 1967, The system diopside-akermanite-nepheline: American Mineralogist, v. 52, p. 227–243.

Pan, Vivian, and Longhi, John, 1987, Low pressure phase equilibria of alkali basalts: Eos, Transactions, American Geophysical Union, v. 68, p. 1542.

Presnall, D. C., 1986, An algebraic method for determining equilibrium crystallization and fusion paths in multicomponent systems: American Mineralogist, v. 71, p. 1061–1070.

Sack, R. O., Walker, D., and Carmichael, I. S. E., 1987, Experimental petrology of alkalic lavas: constraints on cotectics of multiple saturation in natural basic liquids: Contributions to Mineralogy Petrology, v. 96, p. 1–23.

Schairer, J. F., and Bowen, N. L., 1956, The system $Na_2O–Al_2O_3–SiO_2$: American Journal of Science, v. 254, p. 129–195.

Schairer, J. F., and Yoder, H. S., Jr., 1960, The nature of residual liquids from crystallization, with data on the system nepheline-diopside-silica: American Journal of Sci., v. 258-A, p. 273–283.

———— 1961, Crystallization in the system nepheline-forsterite-silica at one atmosphere; Carnegie Institution Washington Yearbook 1960, p. 141–144.

———— 1964, Crystal and liquid trends in simplified alkali basalts; Carnegie Institution Washington Yearbook 1963, p. 65–74.

Yoder, H. S., Jr., and Schairer, J. F., 1968, The melilite-plagioclase incompatibility dilemma in igneous rocks; Carnegie Institution Washington Yearbook 1967, p. 101–103.

Yoder, H. S., Jr., and Tilley, C. E., 1962, Origin of basalt magmas: an experimental study of natural and synthetic rock systems; Journal Petrology, v. 3, p. 342–532.